Available online at www.sciencedirect.com
ScienceDirect
Trans. Nonferrous Met. Soc. China 22(2012) 2379−2388
Transactions of Nonferrous Metals Society of China
www.tnmsc.cn

High temperature tensile properties of laser butt-welded plate of Inconel 718 superalloy with ultra-fine grains

QU Feng-sheng[1], LIU Xu-guang[1], XING Fei[1], ZHANG Kai-feng[2]

1. School of Materials Science and Engineering, Chongqing University, Chongqing 400044, China;
2. College of Materials Science and Engineering, Harbin Institute of Technology, Harbin 150001,China

Received 9 July 2012; accepted 8 August 2012

Abstract: For successfully forming multi-sheet cylinder sandwich structure of Inconel 718 superalloy, high temperature tensile properties of laser butt-welded plate of Inconel 718 superalloy were studied. The experiment results show that tensile direction has great effect on elongation of the laser butt-welded plate. Under conditions of transverse direction tension, the maximum elongation reaches 458.56% at 950 °C with strain rate of 3.1×10^{-4} s^{-1}, in which the strain rate sensitivity value m is 0.352 and the welding seam is not deformed. Under conditions of longitudinal direction tension, the maximum elongation is 178.96% at 965 °C with strain rate of 6.2×10^{-4} s^{-1}, in which m-value is 0.261, and the welding seam contributes to the deformation with the matrix. The microstructure in as-welded fusion zone is constituted of austenite dendrites and Laves phase precipitated in interdendrites. After longitudinal direction tension, a mixed microstructure with dendrite and equiaxed crystal appears in the welding seam due to dynamic recrystallization. After high temperature deforming, many δ-phase grains are transformed from Laves phase grains but a small part of residual Laves phase grains still exist in the welding seam. The deformation result of multi-sheet cylinder sandwich structure verifies that high temperature plasticity of the laser butt-welded plate can meet the requirement of superplastic forming.
Key words: Inconel 718 alloy; laser welding; high temperature plasticity; microstructure

1 Introduction

Inconel 718, an aging hardening Ni−Cr−Fe superalloy, has perfect mechanical properties, excellent anti-fatigue performance and corrosion resistance below 650 °C [1,2]. Therefore, it is widely used for aviation, aerospace, petroleum, chemicals, energy and other fields [3]. Multi-sheet cylinder sandwich structures of Inconel 718 superalloy are important heat resisting and shielding structures in high-speed vehicle [4]. However, the severe tendency of strain hardening of Inconel 718 alloy limits the sheet size to meet the size for multi-sheet cylinder sandwich structures [5]. The bending plate and butt-welding technology can make the small-size sheet splice the heavy-size sheet with homogeneous thickness of wall and shorter manufacturing cycle. Thus the high temperature plasticity of Inconel 718 superalloy with butt-welding seam has great influence on the manufacture of multi-sheet cylinder sandwich structure. In recent years, research works on laser butt-welded plate of Inconel 718 superalloy have been focused on the effect of heat treatment process on the microstructures and mechanical properties of the welded seam [1,6,7]. JANAKI RAMA et al [6] studied the microstructure and tensile properties of Inconel 718 pulsed Nd-YAG laser welds by heat treatment technology. GAO et al [7] studied the microstructures and high temperature mechanical properties of electron beam welded Inconel 718 superalloy thick plate, and the temperature of mechanical test was 650 °C. And the research works on superplasticity of a laser-welded Ti-alloy joint were reported [8−10]. There are few reports about high temperature plasticity and microstructures development of laser butt-welded plate of Inconel 718 superalloy beyond 900 °C. In this work, the high temperature tensile properties and microstructures development from 950 °C to 980 °C for laser butt-welded plate of Inconel 718 superalloy were studied. At last, the experiment results were applied to fabrication of the multi-sheet cylinder sandwich structure of Inconel 718 superalloy.

Foundation item: Project (20102302120002) supported by the Research Fund for the Doctoral Program of Higher Education of China
Corresponding author: QU Feng-sheng; Tel: +86-23-18696586956; E-mail: qufengsheng@163.com
DOI: 10.1016/S1003-6326(11)61474-X

2 Experimental

Test material was Inconel 718 superalloy sheet with ultra-fine grains. The process for the ultra-fine grains: (1050 °C, 0.5 h) with successive water quenching, 50% cold rolling + (890 °C, 10 h) δ-phase precipitation treatment+30% cold rolling+(950 °C, 3 h) recrystallization annealing. The grain size is ASTM13−14 as shown in Fig. 1. The chemical composition is listed in Table 1.

Table 1 Chemical composition of Inconel 718 alloy (mass fraction, %)

C	Si	Mn	Ni
0.067	0.08	0.03	53.32
Cr	Fe	Co	Ti
19.26	16.42	0.05	1.13
Al	Mo	Nb	S
0.55	3.26	5.73	0.005
P	Mg	Cu	B
0.008	<0.01	0.072	0.006

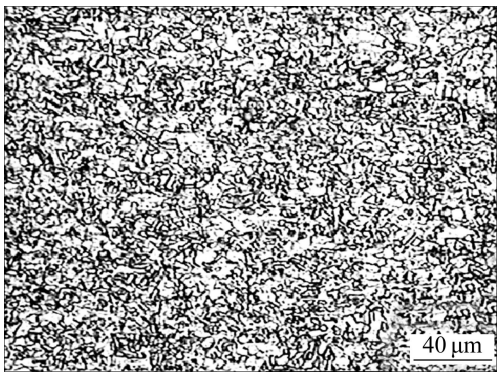

Fig. 1 Microstructure of Inconel 718 superalloy with ultra-fine grains

The laser butt-welding of Inconel 718 superalloy was carried out in a cross-flow CO_2 continuous laser generator (DC030−type), by the means of one-side welding with two-side formation technology. The welding parameters of Inconel 718 superalloy are listed in Table 2. High temperature deformation was carried out in an Instron5500R universal testing machine with an electrical resistance furnace with error less than ±0.1 °C. The high temperature tensile tests were conducted in two tensile directions: transverse direction and longitudinal direction, as shown in Fig. 2. The *m*-values were measured in a Gleeble−1500 thermal simulation testing machine by Backfen's method. The microstructures of welded joint and base metal before and after tension were investigated by an OLYMPNS-GX51 optical microscope and an FEI QAUANTA 2000 scanning electron microscope. Element contents of precipitated phases and dendrites in the weld fusion were estimated by image analysis software.

Table 2 Laser butt-welding parameters of Inconel 718 superalloy with ultra-fine grain

Power/W	Welding speed/ ($mm \cdot min^{-1}$)	Defocusing amount/mm	Shielding gas/($L \cdot min^{-1}$)
900	1400	−1	0.6

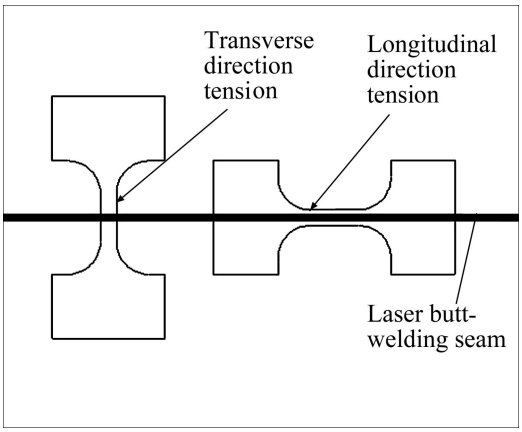

Fig. 2 Schematic diagram of Inconel 718 butt-welded plate tensile test

3 Results and discussion

3.1 High temperature tensile properties of laser butt-welded plate

Specimens after high temperature tension at 950−980 °C with strain rate of 3.1×10^{-4} s^{-1} are shown in Figs. 3(a) (transverse direction) and (b) (longitudinal direction). Curves of elongation—stress in transverse and longitudinal directions are shown in Figs. 4(a) and (b), respectively. The values of elongation, peak flow stress and strain rate sensitivity(*m*-value) and thickness of the weld seam are listed in Table 3.

It can be seen from Fig. 3(a) that the specimens exhibit bamboo-shape after transverse direction tension and the *m*-values are all higher than 0.3. When the *m*-value is higher than 0.3 or the elongation is over 200%, the material exhibits superplasticity [11]. It is conducted that the deformation in this experiment is located at base material rather than welding seam, and this indicates that the strength of welding seam is higher than that of base metal in the test. From Fig. 1, it can be seen that the grains in base material are with grain size of ASTM13−14, which has superplasticity under the test condition. The major deformation mechanism is grain boundary sliding, with the coordination of dislocation slip [5]. But in the laser welding seam, it is as-cast microstructure in non-equilibrium state and Laves phase

distributes in interdendritic region of fusion interior and boundary, and the details will be discussed in Section 3.2. The as-cast microstructure at the welding seam cannot meet the superplasticity requirement of equiaxed grain size lower than 10 μm for Inconel 718 alloy. It cannot exhibit the extremely low flow stress as that with superplasticity. In addition, Laves phase occurring in microstructures of the welding seam increases the flow stress in the welding seam. This is because Laves phase is a topologically close-packed phase with high-temperature strength and high creep resistance, which makes the flow stress in welding seam higher than that of the base metal and increases the creep resistance of the welding seam. In Fig. 3(b), it shows that under the conditions of longitudinal direction tension, welding seam and base material contribute to deformation. And the specimens do not exhibit the bamboo-shape but neck down. From Fig. 3(b) and Fig. 4(b), it shows that the elongation

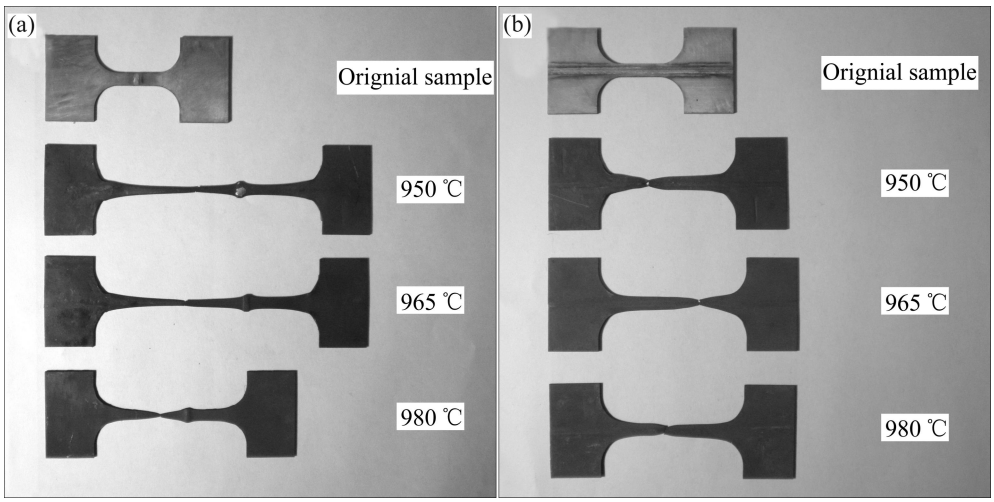

Fig. 3 Specimens in tensile test at different temperatures with strain rate of 3.1×10^{-4} s^{-1}: (a) Transverse direction tension; (b) Longitudinal direction tension

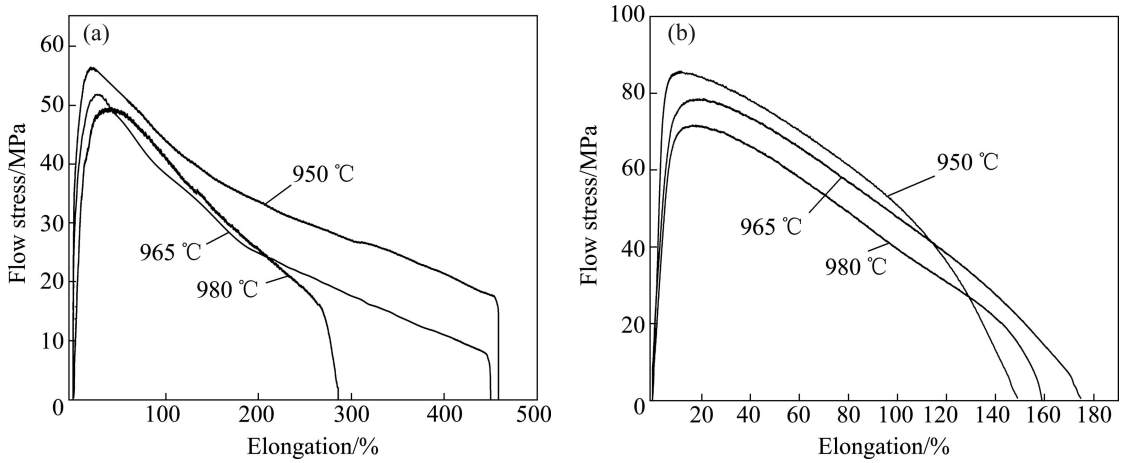

Fig. 4 Curves of elongation—flow stress of specimens with strain rate of 3.1×10^{-4} s^{-1} at different temperatures: (a) Transverse direction tension; (b) Longitudinal direction tension

Table 3 Values of elongation, peak flow stress and *m* of specimens with strain rate of 3.1×10^{-4} s^{-1} at different temperatures

Tensile mode	Deforming temperature/°C	Elongation/%	Peak flow stress/MPa	*m*-value	Thickness of weld seam/mm
Transverse direction	950	458.56	56.47	0.352	3.05
	965	450.12	51.82	0.346	3.02
	980	285.92	49.60	0.318	3.06
Longitudinal direction	950	148.96	85.70	0.237	2.03
	965	174.78	78.56	0.252	1.86
	980	158.95	71.70	0.247	1.92

dramatically reduces but the flow stress significantly increases under the conditions of longitudinal direction tension. This is because the geometric position of the welding seam leads to the welding seam deforming. As shown above, the welding seam cannot exhibit superplasticity, which leads to the elongation decreasing and the flow stress increasing. And these states can be validated by the flow stress, *m*-value and thickness of the welding seam.

Photos of tensile specimens at 965 °C with different strain rates in transverse and longitudinal direction tensions are shown in Figs. 5(a) and (b), respectively. And Table 4 shows values of the elongation, peak flow stress, *m* and thickness of the welding seam. From Table 4, it can be seen that within the range of strain rate of 3.1×10^{-4}−1.8×10^{-3} s^{-1} in transverse direction tension, the values of elongation are over 260%, and *m*-values are higher than 3.0. With the strain rate increasing, the flow stress increases but the elongation decreases. In addition, the flow stress in the welding seam is higher than that of

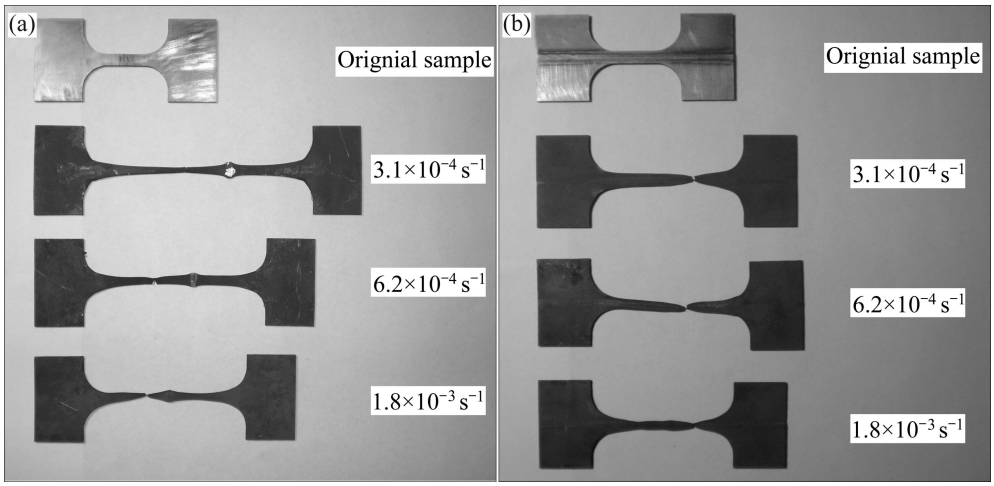

Fig. 5 Tensile specimens at 965 °C with different strain rates in transverse direction tension (a) and longitudinal direction tension (b)

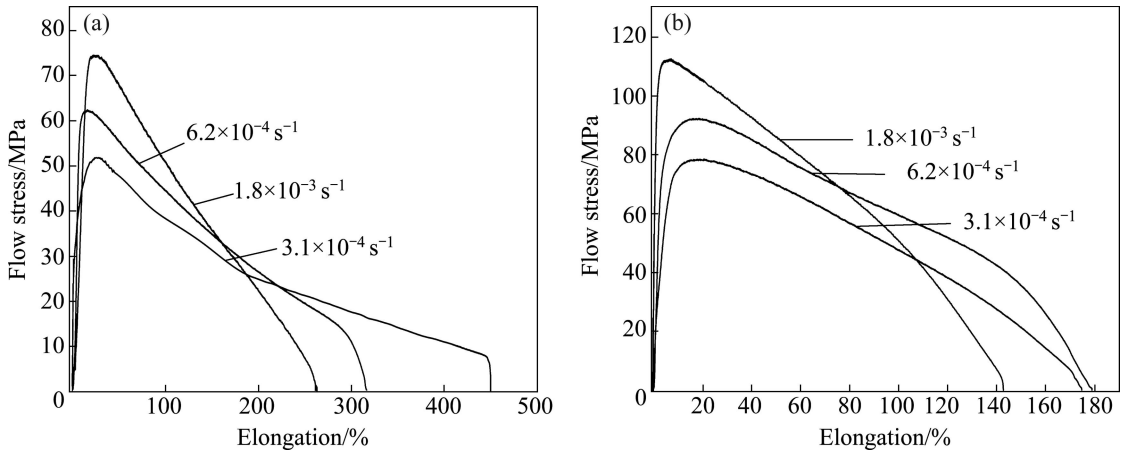

Fig. 6 Curves of elongation—flow stress of specimens at 965 °C with different strain values in transverse direction tension (a) and longitudinal direction tension (b)

Table 4 Values of elongation, peak flow stress and *m* of Inconel 718 superalloy in tension at 965 °C with different strain rates

Tensile mode	Strain rate /s^{-1}	Elongation/%	Peak flowing stress/MPa	*m*-value	Thickness of weld seam/mm
Transverse direction	3.1×10^{-4}	450.12	51.82	0.346	3.01
	6.2×10^{-4}	316.70	62.40	0.327	3.02
	1.8×10^{-3}	263.26	74.50	0.308	3.04
Longitudinal direction	3.1×10^{-4}	174.78	78.56	0.252	1.86
	6.2×10^{-4}	178.96	92.40	0.261	1.90
	1.8×10^{-3}	142.82	112.60	0.223	1.98

base material. For longitudinal direction tension, the largest elongation reaches 178.96% at the strain rate of 6.2×10^{-4} s^{-1}. The flow stress increases with the strain rate increasing.

The test results show that at 965 °C and in the range of strain rate 3.1×10^{-4}−6.2×10^{-4} s^{-1}, the butt-welded plate exhibits excellent superplasticity, which can meet the forming requirements of the part.

3.2 Effect of high temperature tension on microstructures evolution

3.2.1 Microstructures of as-welded seam

Figure 7 shows the microstructures of fusion zone in as-welded specimens. It is found that the dendrites in fusion interior are fine and equiaxed with grain size of ASTM15−16 (Fig. 7(a)), and at region adjacent to the fusion boundary, the dendrites are slightly coarser and columnar with grain size of ASTM8−9 ((Fig. 7(b)). According to the theory of morphological stability originally developed by MULLINS and SEKERKA [12], the temperature gradient (G) and the growth rate (R) are very important factors for determining the solidification morphology and grain size. The thermal gradients in a weld pool are steeper at regions close to fusion boundary than those in weld interior. The steeper thermal gradient prevailing at the fusion boundary is responsible for the columnar dendrite growth in a direction opposite to the heat extraction direction. Towards the weld center, however, the thermal gradient is not as steep, which in combination with the very rapid cooling rates of laser beam welding, results in significant undercooling (low G/R), leading to the formation of fine equiaxed dendrites. The gain size in heat affected zone (HAZ) grows gently to ASTM10−11 due to heat input in laser welding, as shown by the arrow in Fig. 7(b).

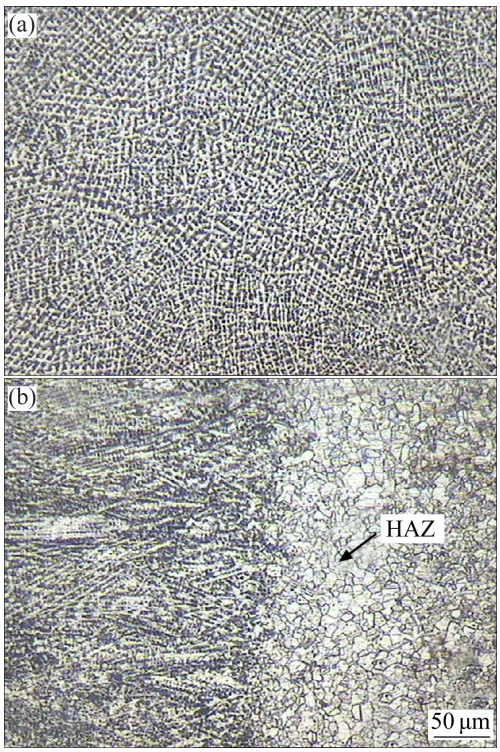

Fig. 7 Microstructures of fusion zone (as-welded condition): (a) Very fine equiaxed dendrites in weld interior; (b) Columnar dendrites adjacent to fusion boundary

The SEM microstructures of the weld fusion zone are shown in Figs. 8(a) (at weld center) and (b) (adjacent to fusion boundary). A number of precipitated phases occur in the weld fusion zone. The precipitated phases in the weld center distribute discretely. But the distribution of precipitated phases adjacent to the fusion boundary is slightly regular and directional. The element contents of dendrite and precipitated phase in weld joint measured by the EDAX spectrum analysis are listed in Table 5. From Table 5, it can be seen that the precipitated phase is rich in Nb, Mo and Ti, and poor in Ni, Cr and Fe, compared with the base material. The dendrite core is

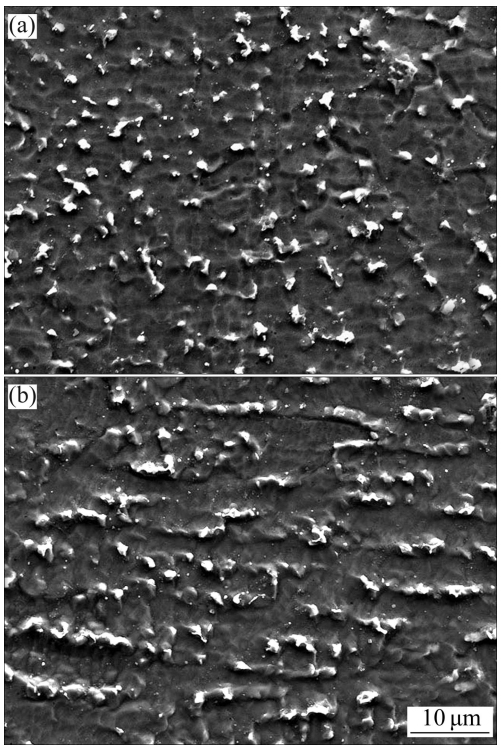

Fig. 8 SEM microstructures of fusion zone (as-welded condition): (a) In weld interior showing fine discrete Laves particles; (b) Showing a certain ordination Laves particles adjacent to fusion boundary

Table 5 Element content of dendrite and precipitated phase in weld joint

Phase	Mass fraction/%						
	Ni	Fe	Cr	Nb	Mo	Ti	Al
Dendrite	54.63	19.16	19.51	2.82	2.72	0.65	0.51
Precipitate	48.55	14.39	16.40	14.58	3.82	1.49	0.78

poor in Nb, Ti and Al. The element fraction characteristic shows that the precipitated phase is Laves phase which presents in the cast and welded products of Inconel 718 superalloy. Inconel 718 superalloy is precipitation strengthened primarily by γ'' (Ni_3Nb). The sluggish ageing kinetics of γ'' precipitation is also found to be beneficial to material's weldability [13]. However, since niobium is a high concentration refractory element, it tends to segregate during the solidification process, as a result of the fact that some desirable phase, like Laves phase [13], can form in the welding fusion. Laves phase is a hexagonally close packed phase in the form (Ni, Fe, $Cr)_2$ (Nb, Mo, Ti). And the forming process can be expressed by the following formulations (1) and (2) [14].

$$\text{Liquid} \longrightarrow \text{Liquid enriched with Nb}+\gamma \quad (1)$$

$$\text{Liquid enriched with Nb} \longrightarrow \gamma + \text{Laves} \quad (2)$$

Laves phase is a brittle intermetallics and is topologically close-packed phase. For Inconel 718 supperalloy, the atoms with larger radius are Nb, Ti and Mo, and the minor ones are Fe, Ni and Cr. The crystal structures are complicate, and the coordination numbers reach 14−16 [15]. Laves phase provides the conditions for nucleation and crack growth, which severely impairs the plasticity of Inconel 718 at room temperature. A small amount of granular or small block Laves phase existing in Inconel 718 has little influence on mechanical properties; however, when the content of Laves phase is over 2%−3%, it harms the strength and plasticity of the alloy at room temperature, and impairs 20% strength and 60% plasticity [15]. At 650 °C and 620 MPa, the rupture life and rupture elongation are reduced by 60%, which exhibits the weakening effect of Laves phase. Furthermore, Laves phase occupies plenty of Mo, Ti and Ni, which can also affect the solid solution strengthening and decrease the number of γ'' and γ' to weak the effect of precipitation strengthening. From the analysis of Laves phase in the welding seam, it can be found that there are (5.0±0.4)% Laves phase in the welding seam. In addition, Laves phase has high strength and high creep resistance at high temperature [16]. For instance, the yield strength of $NbCr_2$ at 1200 °C reaches 600 MPa. And this is the key reason why the welding seam is free from deformation in transverse direction tension and the flow stress in longitudinal direction tension remarkably increases.

3.2.2 Microstructures in welding seam after high temperature tension

Metallographic structures of weld interior and boundary in transverse direction tension at 965 °C, strain rate of 3.1×10^{-4} s^{-1} are shown in Figs. 9(a) and (b). From Figs. 9(a) and (b), the grains in welding seam are still dendritic, but grow a little. The grain size in weld interior is ASTM13−14 and a small part is ASTM11, and the columnar crystals in fusion boundary are coarser than grain size of ASTM6 because high temperature improves atomic activity. In addition, the grains in heat affected zone grow up with grain size of ASTM10. Microstructures of weld interior and boundary in longitudinal direction tension at 965 °C and strain rate of 3.1×1^{-4} s^{-1} are shown in Figs. 9(c) and (d). Compared with Figs. 9(a) and (b), the microstructures in longitudinal direction tension change more obviously and the equiaxed grains with grain size of ASTM10 occur in welding seam, as shown by arrow. This is because the microstructures of the welding seam cannot perform superplasticity under the condition of longitudinal direction tension. During the high temperature deformation, on one hand, the dislocation density increases, on the other hand, the forming of subgrains resulting from dislocation dipole cancels, and the polygonization of dislocation cell wall and subgrains merging are conducted by thermal activation. For nickel alloy, a low stacking fault energy metal, it has large extended dislocation width which leads to difficulty to gather characteristic dislocation. Therefore, there is rarely cross-slip dislocation and climbing dislocation. The dynamic recrystallization occurs till the dislocation accumulating to a certainty degree. Thus, the equiaxial grains will occur at fusion zone after longitudinal direction tension.

The microstructures of specimens in fracture are shown in Fig. 9(e). The grains in fracture at fusion zone are almost equiaxial and the cavities occur. This is because in high temperature tension, the dynamic recrystallization performs continuously resulting in a large number of equiaxial grains. The transformation from Laves phase to δ phase at grain boundary is shown in Fig. 10, and the residual Laves phase grains prevent the growth of equiaxial grains. With a larger deformation, especially the strain rate increasing at fracture leads to the crystallization nuclei for dynamic recrystallization increasing, and generates a large number of fine grains. The fine exquiaxed grains provide the possibility of superplasticity. And at the strain rate of 3.1×10^{-4} s^{-1}, the fine equiaxed grains lead to boundary sliding, which is the main deformation mechanism of superplasticity in Inconel 718 superalloy. In addition, the larger flow stress in longitudinal direction tension leads to the strain rate increasing near the fracture. This results in the cavities increasing, and when the cavities are continuous, the specimen fractures. Moreover, the place where Laves phase grains occur and δ phase grains precipitate at the welding seam supplies nucleation and growth of the cavities.

Figures 10(a) and (b) show the microstructures in weld interior and adjacent to boundary in transverse direction tension at 965 °C and strain rate of 3.1×10^{-4} s^{-1}, respectively. From Figs. 10(a) and (b), it can be seen that

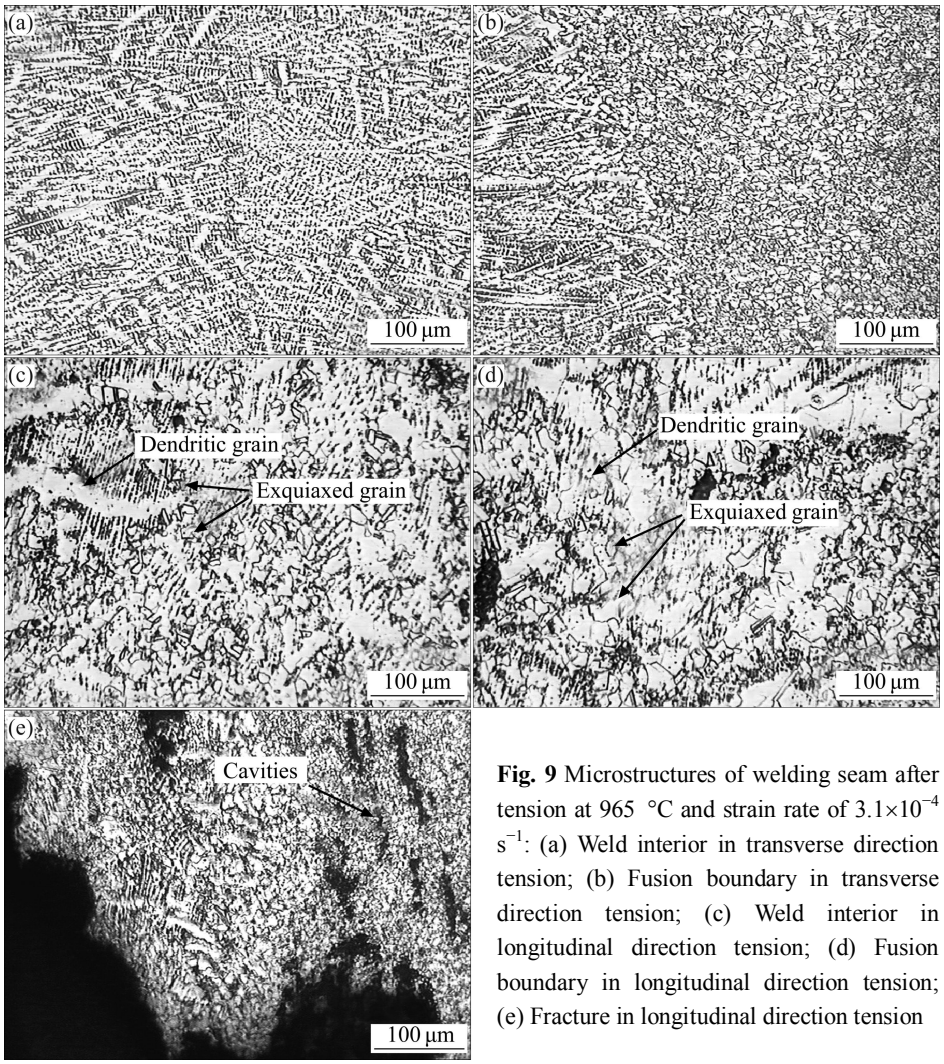

Fig. 9 Microstructures of welding seam after tension at 965 °C and strain rate of 3.1×10^{-4} s^{-1}: (a) Weld interior in transverse direction tension; (b) Fusion boundary in transverse direction tension; (c) Weld interior in longitudinal direction tension; (d) Fusion boundary in longitudinal direction tension; (e) Fracture in longitudinal direction tension

respectively. From Figs. 10(a) and (b), it can be seen that the morphology of precipitated phases changes a lot and there are a number of needle-like precipitated phases in the welding seam, with a spot of residual globosity phase. The microstructures of the weld fusion zone in longitudinal direction tension at 965 °C and strain rate of 3.1×10^{-4} s^{-1} are shown in Figs.10(c) (at weld center) and (d) (at region adjacent to fusion boundary). In addition, the equiaxed grains in longitudinal direction tension can be obviously found. And the elements in dendrite, needle-like precipitated phase and globosity precipitated phase can be obtained by EDAX, as shown in Figs. 10(a), (b) and (c), respectively. Table 6 shows the element contents of the dendrite, needle-like and globosity precipitated phases by EDAX analysis. From the results of EDAX spectrum, the Nb content of the dendrite in the weld fusion zone increases to 4.83%. The Nb content is 5.73% in base material, and the Nb content of needle-like precipitated phase in the weld fusion is 8.03%. This indicates that the precipitated phase is δ phase. The δ phase (Ni_3Nb) with orthogonal and ordered structure is stable phase of the metastable phase γ'' and precipitates in the temperature range of 860−995 °C [5]. The precipitation of δ phase at grain boundary can prevent the growth of grains in Inconel 718 alloy and promote fine and uniform grains, which increase the strengthening and toughening of the alloy. In addition, an appropriate amount of δ phase is in favor of eliminating sensitivity of the nick. In the weld metal solidification, the interdendritic regions become rich in Nb with the Nb content in the range of 6%−10% or more, and the Nb content in regions where Laves phase grains form is more than 10%. Thus, at the end of solidification, there will be the regions around Laves phase grains in the weld metal with sufficient Nb content where δ phase grains can precipitate. However, the rapid cooling rates through the δ phase precipitation range during welding metal preclude the δ phase precipitation from these regions. As shown in Fig. 10, a majority of Laves phase grains transform to needle-like δ phase grains because of enough forming time for δ phase precipitation in high temperature tension. Firstly, δ phase grains precipitate

around Laves phase grains which are rich in Nb element. And then the residual Nb element diffuses to the dendrites, which can also relieve segregation of Nb. By analyzing element contents in Table 6, it shows that the globosity phase is still Laves phase. This is attributed to the fact that whether Laves phase can be dissolved easily or difficultly depends on its Nb content and particle size. Coarser Laves phase grains with higher Nb content require higher temperature and longer soaking time for dissolution. The tensile direction has no influence on the contents of phases and elements. With the analysis by image software, the content of Laves phase in welding seam is 0.8%±0.07% after tension, which is within the safety range. The content of δ phase in transverse direction tension is 7.0%−8.3%, and in longitudinal direction tension is 6.4%−6.9%. The content of δ phase is decreased by deformation.

3.2.3 Microstructures of base material after tension

The microstructures of base material after high temperature tension at strain rate of 3.1×10^{-4} s^{-1} are shown in Figs. 11(a) (at 965 °C in transverse direction tension) and (b) (at 965 °C in parallel welding seam tension), respectively. Compared with microstructures of base material before high temperature tension, the grains of base material after high temperature tension grow gently, and the grain size is ASTM12−13, and the cavities appear in the base material. In general, the cavities occur at grain boundary and phase boundary during the superplastic deformation. And the temperature for tensile test is within the temperature range of precipitation of δ phase. On one hand, δ phase at grain boundary can prevent the growth of the grain; on the other hand, when the grain boundary slides, the particles at the boundary will not coordinate and lead to a large number of cavities. The microstructures of base material at 965 °C and strain rate of 3.1×10^{-4} s^{-1} are shown in Figs. 12(a) (in transverse direction tension) and (b) (in longitudinal direction tension), respectively. In two situations, a large number of cavities are formed. The experiment results were applied to fabrication of multi-sheet cylinder sandwich structure of Inconel 718 superalloy. The photos of the application are shown in Fig. 13.

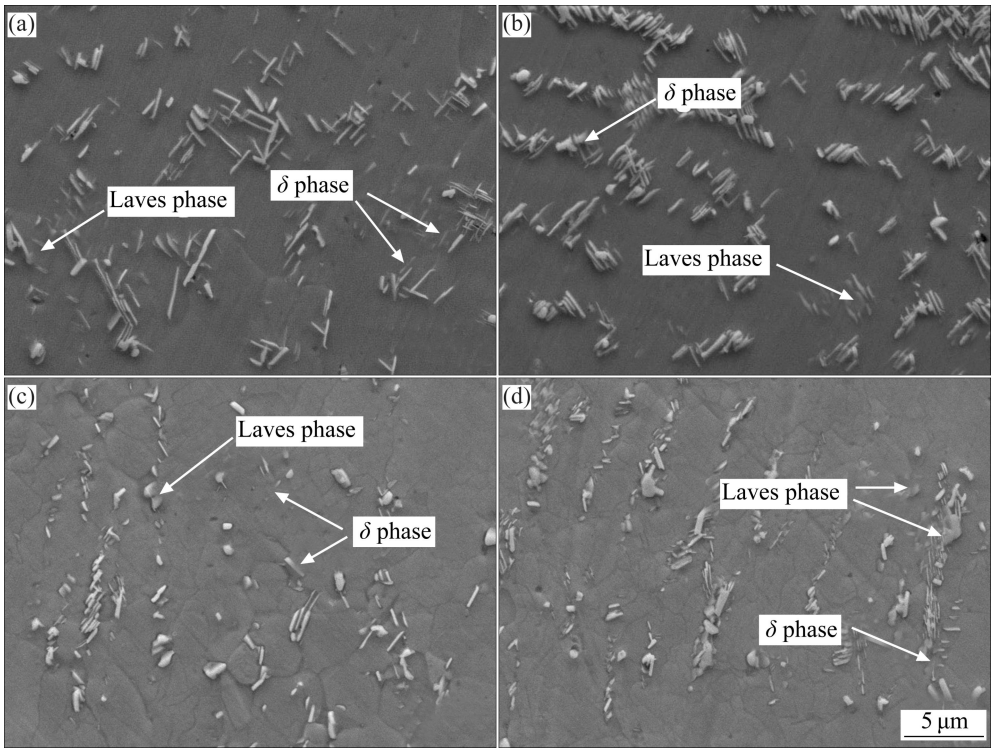

Fig.10 SEM images of base material after tension at 965 °C and 3.1×10^{-4} s^{-1}: (a) Weld interior in transverse direction tension; (b) Weld boundary in transverse direction tension; (c) Weld interior in longitudinal direction tension; (d) Weld boundary in longitudinal direction tension

Table 6 Elements content of dendrite, precipitated phase after superplastic tension

Phase	Mass fraction/ %						
	Ni	Fe	Cr	Nb	Mo	Ti	Al
Dendrite	53.04	18.24	18.65	4.83	3.42	1.11	0.6
Needle-like precipitated phase	52.23	16.94	17.01	8.03	2.84	1.48	0.49
Spherical precipitated phase	47.51	15.86	15.63	14.73	3.94	1.67	0.66

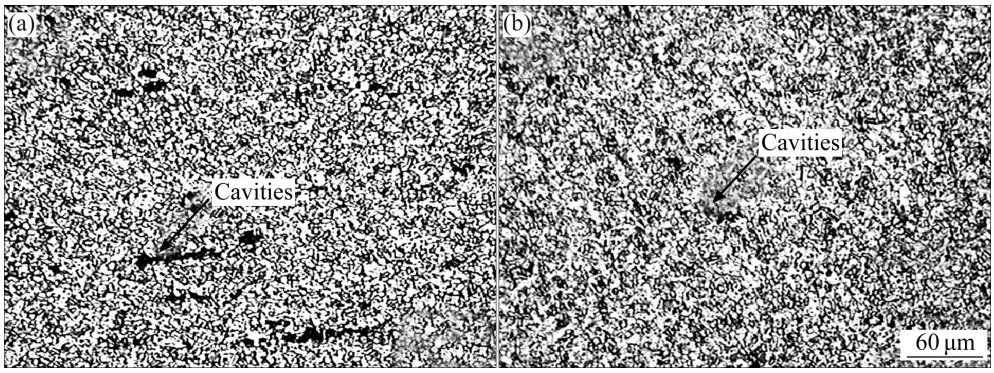

Fig. 11 Microstructures of base material after tension at strain rate of 3.1×10^{-4} s^{-1}: (a) At 965 °C in transverse direction tension; (b) At 965 °C in longitudinal direction tension

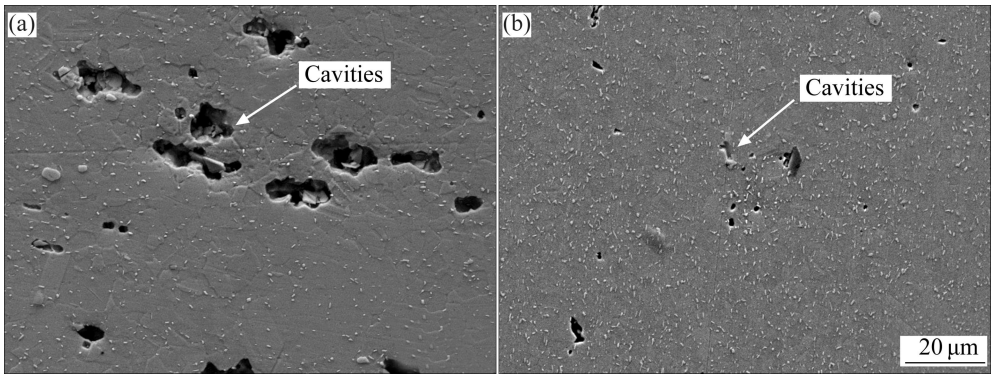

Fig. 12 SEM images of microstructures of base material at strain rate of 3.1×10^{-4} s^{-1} at 965 °C: (a) In transverse direction tension; (b) In longitudinal direction tension

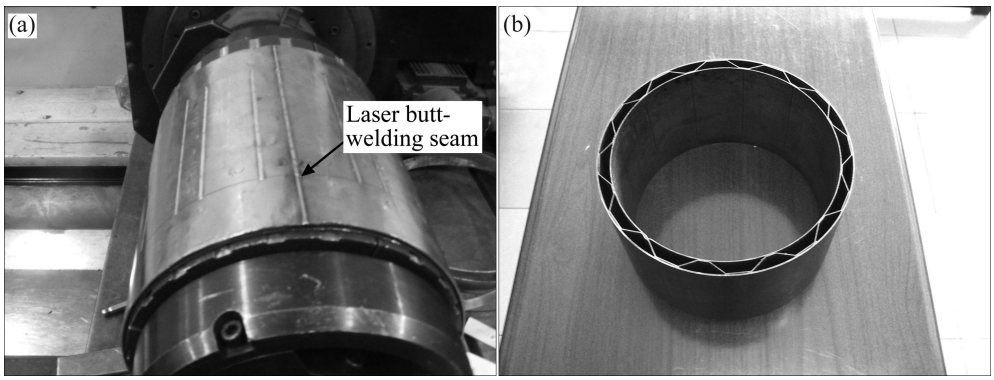

Fig. 13 Application in multi-sheet cylinder sandwich structure of Inconel 718 superalloy: (a) Welding seam; (b) Top view of product

4 Conclusions

1) In transverse direction tension performed in temperature range of 950 °C−980 °C and strain rate of 3.1×10^{-4} s^{-1}, the largest elongation of laser butt-welded plate is 458.56% at 950 °C, with a unique deformation region in base material. In longitudinal direction tension, the elongation reduces dramatically but the flow stress increases significantly. The largest elongation of 178.96% occurs at 965 °C and strain rate 3.1×10^{-4} s^{-1}. The flow stress of the welding seam is higher than that of base material in the experiments.

2) The dendrites in as-welded welding interior are fine and equiaxed but in region adjacent to fusion boundary are coarser and columnar. And there are Laves phase grains formed in welding process.

3) The microstructures of the welding seam in transverse direction tension at 965 °C and strain rate 3.1×10^{-4} s^{-1} preserve the characteristics in as-welded material, with a little growth. Under the same condition in longitudinal direction tension, the equiaxed grains form due to the dynamic recrystallization. In addition, a majority of Laves phase grains in the welding seam is transformed to δ phase grains after high temperature tension. Therefore, deformation is favorable to improving

the microstructures of the welding seam.

4) The cavities are formed in deformation of base material because the superplastic deformation mechanism of base material is grain boundary sliding, which leads to the formation of the cavities.

References

[1] SGOBBI S, ZHANG L, NORRIS J, RICHTER K H , LOREAU J H. High powder CO_2 and Nd−YAG laser welding of wrought Inconel 718 [J]. Journal of Materials Process Technology, 1996, 56: 333−345.

[2] WANG Yan, SHAO Wen-zhu, ZHEN Liang. Dissolution behavior of δ phase and its effects on deformation mechanism of GH4169 alloy [J]. The Chinese Journal of Nonferrous Metals, 2011, 21(2): 341−342.(in Chinese)

[3] KONG Yong-hua, HU Hua-bin, LI Long, CHEN Guo-sheng, ZHU Shi-gen. Study on the microstructures and properties of GH4169 alloy by different forging technology [J]. Rare Metal Materials and Engineering, 2011, 40(S2): 225−226. (in Chinese)

[4] QU Feng-sheng, LU Zhen, XING Fei, ZHANG Kai-feng. Study on LBW/SPF technology of multi-sheet cylinder sandwich structure for inconel 718 Superalloy [J]. Journal of Sichuan University: Engineering Science Edition, 2102,44(3): 185−186. (in Chinese)

[5] LU Hong-jun. Study of untra-fine grain processing and superplastic forming of GH4169 superalloy sheet [D]. Harbin: Harbin Institute of Technology, 2003. (in Chinese)

[6] JANAKI RAMA G.D, ENUGOPAL REDDYA A V, PRASAD RAOB K, REDDYC G M, SARIN SUNDAR J K. Microstructure and tensile properties of Inconel 718 pulsed Nd-YAG laser welds [J]. Journal of Material Processing Technology, 2005, 167: 73−82.

[7] GAO Peng, ZHANG Kai-feng, ZHANG Bing-gang, JIANG Shao-song, ZHANG Bao-wei. Microstructures and high temperature mechanical properties of electron beam welded Inconel 718 superalloy thick plate [J]. Transactions of Nonferrous Metals Society of China, 2011, 21: s315−s322.

[8] CHEN S H, HUANG J H, CHENG D H, ZHANG H, ZHAO X K. Superplastic deformation mechanism and mechanical behavior of a laser-welded Ti−6Al−4V alloy joint [J]. Materials Science and Engineering A, 2012, 541: 110−119.

[9] CHENG Dong-hai, HUANG Ji-hua, CHEN Yi-ping, HU De-an. Microstructure evolution characterization of weld joints by laser welding for superplastic deformation of titanium alloy [J]. Rare Metal Materials and Engineering, 2012, 41(2): 368−371. (in Chinese)

[10] CHENG Dong-hai, HUANG Ji-hua, LIN Hai-fan, ZHAO Xing-ke, ZHANG Hua. Superplastic deformation behavior and microstructures of laser welded titanium alloy [J]. The Chinese Journal of Nonferrous Metals, 2010, 20(1): 67−71. (in Chinese)

[11] WEN Jiu-ba, YANG Yun-lin, YANG Yong-shun, CHEN Fu-xiao, ZHANG Ke-ke, ZHANG Yao-zong. Application of superplasticity technology [M]. Beijing: China Machine Press, 2005: 1−2. (in Chinese)

[12] MULLINS W W, SEKERKA R F. Stability of a planar interface during solidification of a dilute binary alloy [J]. Journal of Applied Physics, 1964, 35(2): 444−451.

[13] BISWAS S, REDDY G M, MOHANDAS T, MURTHY V S. Residual stresses in Inconel 718 electron beam welds [J]. Journal of Material Science, 2004, 39: 6813−6815.

[14] RADHAKRISHNA C H, PRASAD R K. The formation and control of Laves phase in superalloy 718 welds [J]. Journal of Material Science, 1997, 32(8):1977−1984.

[15] GUO Jian-ting. Materials science and engineering for superalloys(I) [M]. Beijing: Science Press, 2008: 353−360. (in Chinese)

[16] LEE S B, LIAW P K, LIU C T, CHOU Y T. Cracking in Cr−Cr_2Nb eutectic alloys due to thermal stresses [J].Materials Science and Engineering A,1999, 268(1−2): 184−192.

超细晶 Inconel 718 合金激光对接板的高温拉伸性能

曲凤盛[1]，刘旭光[1]，邢 飞[1]，张凯锋[2]

1. 重庆大学 材料科学与工程学院，重庆 400044;
2. 哈尔滨工业大学 材料科学与工程学院，哈尔滨 150001

摘 要：为使 Inconel 718 合金的筒形多层夹芯结构顺利成形，研究该合金激光对接板的高温塑性。结果表明，拉伸方向对激光对接板的伸长率有很大影响。横向拉伸时，在温度为 950 °C 和应变率为 3.1×10^{-4} s^{-1} 的条件下，最大伸长率为 458.56%，此时 m 值为 0.352，焊缝未变形。纵向拉伸时，在温度为 965 °C 和应变速率为 6.2×10^{-4} s^{-1} 的条件下，最大延长率为 178.96%，此时 m 值为 0.261，焊缝随母材同时变形，焊缝的微观组织为树枝晶，晶间析出了 Nb 含量较高的 Laves 相。纵向拉伸时，由于动态再结晶的缘故，焊缝中出现了由树枝晶和等轴晶组成的混合组织。高温变形后，焊缝中的大量 Laves 相转化为 δ 相，但焊缝中仍有小部分残余的 Laves 相存在。多层夹芯筒结构成形的结果表明，激光对焊板的高温塑性能满足其筒形夹芯结构的要求。

关键词：Inconel 718 合金；激光焊接；高温塑性；微观组织

(Edited by HE Xue-feng)